

Article

An Evaluation of Turbocharging and Supercharging Options for High-Efficiency Fuel Cell Electric Vehicles

Arthur Kerviel ^{1,2}, Apostolos Pesyridis ^{1,*} , Ahmed Mohammed ¹ and David Chalet ²

¹ Department of Mechanical and Aerospace Engineering, Brunel University, London UB8 3PH, UK; Arthur.Kerviel@brunel.ac.uk (A.K.); Ahmed.Mohammed@brunel.ac.uk (A.M.)

² Ecole Centrale de Nantes, LHEEA Lab. (ECN/CNRS), 44321 Nantes, France; david.chalet@ec-nantes.fr

* Correspondence: a.pesyridis@brunel.ac.uk; Tel.: +44-189-526-7901

Received: 17 October 2018; Accepted: 19 November 2018; Published: 3 December 2018



Abstract: Mass-produced, off-the-shelf automotive air compressors cannot be directly used for boosting a fuel cell vehicle (FCV) application in the same way that they are used in internal combustion engines, since the requirements are different. These include a high pressure ratio, a low mass flow rate, a high efficiency requirement, and a compact size. From the established fuel cell types, the most promising for application in passenger cars or light commercial vehicle applications is the proton exchange membrane fuel cell (PEMFC), operating at around 80 °C. In this case, an electric-assisted turbocharger (E-turbocharger) and electric supercharger (single or two-stage) are more suitable than screw and scroll compressors. In order to determine which type of these boosting options is the most suitable for FCV application and assess their individual merits, a co-simulation of FCV powertrains between GT-SUITE and MATLAB/SIMULINK is realised to compare vehicle performance on the Worldwide Harmonised Light Vehicle Test Procedure (WLTP) driving cycle. The results showed that the vehicle equipped with an E-turbocharger had higher performance than the vehicle equipped with a two-stage compressor in the aspects of electric system efficiency (+1.6%) and driving range (+3.7%); however, for the same maximal output power, the vehicle's stack was 12.5% heavier and larger. Then, due to the existence of the turbine, the E-turbocharger led to higher performance than the single-stage compressor for the same stack size. The solid oxide fuel cell is also promising for transportation application, especially for a use as range extender. The results show that a 24-kWh electric vehicle can increase its driving range by 252% due to a 5 kW solid oxide fuel cell (SOFC) stack and a gas turbine recovery system. The WLTP driving range depends on the charge cycle, but with a pure hydrogen tank of 6.2 kg, the vehicle can reach more than 600 km.

Keywords: turbocharger; supercharger; E-turbocharger; Proton-exchange membrane fuel cell; solid oxide fuel cell; range extender

1. Introduction

The Intergovernmental Panel on Climate Change (IPCC) study from 2014 showed that 14% of global greenhouse gas emissions are due to transportation [1]. Since 65% of greenhouse gas emissions are related to CO₂, it has become crucial to decrease their global warming impact. Taking well-to-wheel emissions into consideration, electric vehicles reach 180 g CO₂eq/km (because of a global 68% electricity production still coming from oil, gas, and coal) whereas fuel cell vehicles (FCVs) reach 127 g CO₂ eq/km [2,3]. Even if current regulations only take into account tank-to-wheel emissions, which are null for both of these types of vehicle, some car manufacturers such as Toyota (Mirai), Honda (Clarity Fuel Cell), or Daimler Group (GLC F-cell) are investing in fuel cell technology to

prepare for an uncertain future. To become a viable solution for transportation, fuel cell vehicles must deal with power density challenges. For instance, the Hyundai Tucson Fuel Cell edition is 300 kg heavier than the gasoline version for the same output power. To decrease the weight of the fuel cell vehicle means less fuel consumption, and thus a higher driving range.

There is a large potential for increasing the power density by using a boosting system for the air supply. A higher pressure of air means a higher output power and efficiency. As seen in Figure 1, a recent paper from Honda underlined that increasing the pressure ratio from 1.0 to 1.7 provided 10% more output power [4]. As a consequence, it is possible to reduce the number of cells and thus the weight of the fuel cell stack for the same output power. Given that the requirements differ from those of an internal combustion engine (ICE), the choice of compressor type must be adapted to fuel cell vehicle application.

In order to determine which type of compressor to use, a literary survey was conducted to identify which types of fuel cell are relevant to transportation application. This was followed by the development of fuel cell vehicle powertrain models, employing co-simulation between GT-SUITE and MATLAB/SIMULINK. Finally, simulations have included driving cycle simulations to analyse the impact of the air supply system on vehicle performances.

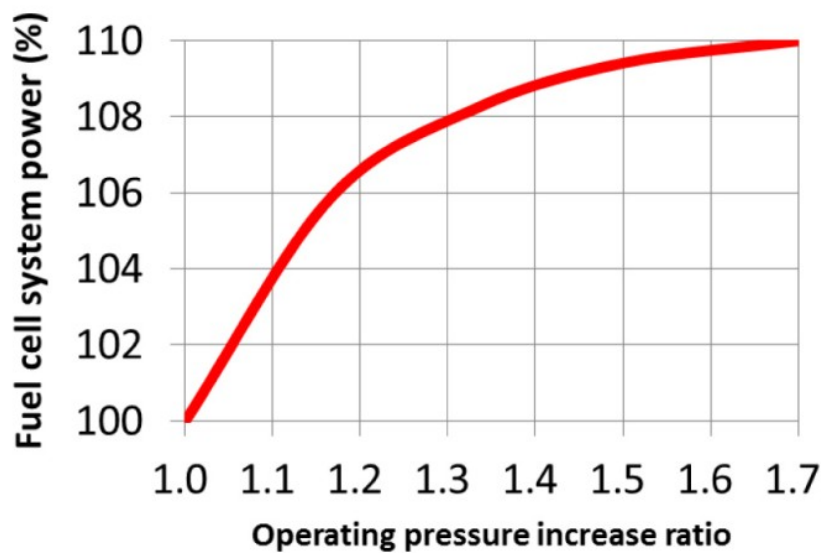


Figure 1. Influence of the operating pressure on the fuel cell output power.

2. Methodology

2.1. Proton Exchange Membrane Fuel Cell (PEMFC) Model

A polarisation curve model has been used to model the operation of a monocell pure hydrogen PEMFC with MATLAB/SIMULINK. The model, which was proposed by Pukrushpan [5], and was used in the MATLAB/SIMULINK environment, is described by the following equations:

$$V_{cell} = E_{nerst} - V_{act} - V_{conc} - V_{ohm} \tag{1}$$

$$E_{nerst} = 1.229 - 0.85 \times 10^{-3}(T - 298.15) + \frac{RT}{2F} \log(P_{H_2} * P_{O_2}^{0.5}) \tag{2}$$

$$V_{act} = v_0 + v_a [1 - \exp(-c_1 * i)] \tag{3}$$

$$V_0 = 0.279 - 0.85 \times 10^{-3}(T - 298.15) + \frac{RT}{2F} \log[(P_{H,in} - P_{sat}) * 0.1173 * (P_{A,in} - P_{sat})^{0.5}] \tag{4}$$

$$V_a = [-1.618 * 10^{-5} * T + 1.168 * 10^{-2}] \left[\frac{P_{O_2}}{0.1173} + P_{sat} \right]^2 + [1.8 * 10^{-4} * T - 0.166] \left[\frac{P_{O_2}}{0.1173} + P_{sat} \right] + [-5.8 * 10^{-4} * T + 0.5736] \quad (5)$$

$$V_{conc} = i * \left(c_2 * \frac{i}{i_L} \right)^{c_3} \quad (6)$$

$$c_2 = [8.66 * 10^{-5} * T - 0.068] \left[\frac{P_{O_2}}{0.1173} + P_{sat} \right] - (1.6 * 10^{-4} * T + 0.54) \quad (7)$$

$$V_{ohm} = R_i * i \quad (8)$$

where V_{cell} is the output tension of the monocell. E_{nerst} is the Nerst potential. V_{act} , V_{conc} and V_{ohm} are respectively the activation, mass transfer, and ohmic losses. $C1$ and $C3$ are given by a recent paper concerning air supply system control [6] as $C1 = 10$ and $C3 = 2$.

The total output power of the N-cells' stack is calculated as:

$$P = N * V_{cell} * I \quad (9)$$

The electrochemical reaction is considered as stoichiometric. The system is supposed to run with an excess of air. The current is calculated from the hydrogen mass flow rate, and the excess of air is included in the calculation of oxygen partial pressure. As a result, the PO_2 and PH_2 from previous equations are calculated by taking the average between the inlet and outlet stack pressure as follows:

$$P_{O_2} = 0.5 * (P_{A,in} * 0.21) * \left(1 + \frac{Dm_{O,out}}{Dm_{O,in}} \right) \quad (10)$$

$$P_{H_2} = 0.5 * P_{H,in} * \left(1 + \frac{Dm_{H,out}}{Dm_{H,in}} \right) \quad (11)$$

where $Dm_{O,in}$ and $Dm_{H,in}$ are the inlet mass flow rates, and $Dm_{O,out}$ and $Dm_{H,out}$ are the outlet mass flow rates of oxygen and hydrogen, respectively. $P_{A,in}$ and $P_{H,in}$ are the inlet pressures of air and hydrogen.

As seen in Figure 2, the MATLAB/SIMULINK model runs as a black box in the GT-SUITE environment. The "PEMFCs_model" refers to the MATLAB function using the model described. The inputs are the inlet mass flow rates ($Dm_{A,in}$, $Dm_{H,in}$), the inlet pressures ($P_{A,in}$, $P_{H,in}$), and the required power by the air supply system (P_{comp}). The outputs include the outlet mass flow rates ($Dm_{A,out}$, $Dm_{H,out}$), the outlet air pressure ($P_{A,out}$), the output produced power, the current, and the electric efficiencies (P , I , R_{eff} , $R_{eff,system}$). There are different ways of calculating the electric efficiency. In this paper, it is the electric stack efficiency and the electric system efficiency that are considered and calculated as follows [4,7,8]:

$$R_{eff} = \frac{P}{1.481 * N * I} \quad (12)$$

$$R_{eff,system} = \frac{P - P_{comp}}{1.481 * N * I} \quad (13)$$

where N is the number of cells, and 1.481 is the theoretical voltage at the terminals of a hydrogen fuel cell.

As seen in Figure 3, the GT-SUITE model takes into consideration the air consumed through the stack. Dm_{eject} is the part of air consumed during the electrochemical reaction. It is used to model the decrease of air mass flow rate through the stack due to the oxygen consumption. $Coeff_pressure$, which is calculated with an equation from GT-SUITE, is used to take into consideration the pressure loss through the stack due to oxygen consumption. The GT-SUITE equation is a simplified model of pressure loss. So, a gain has been added to consider the compressible character of the air.

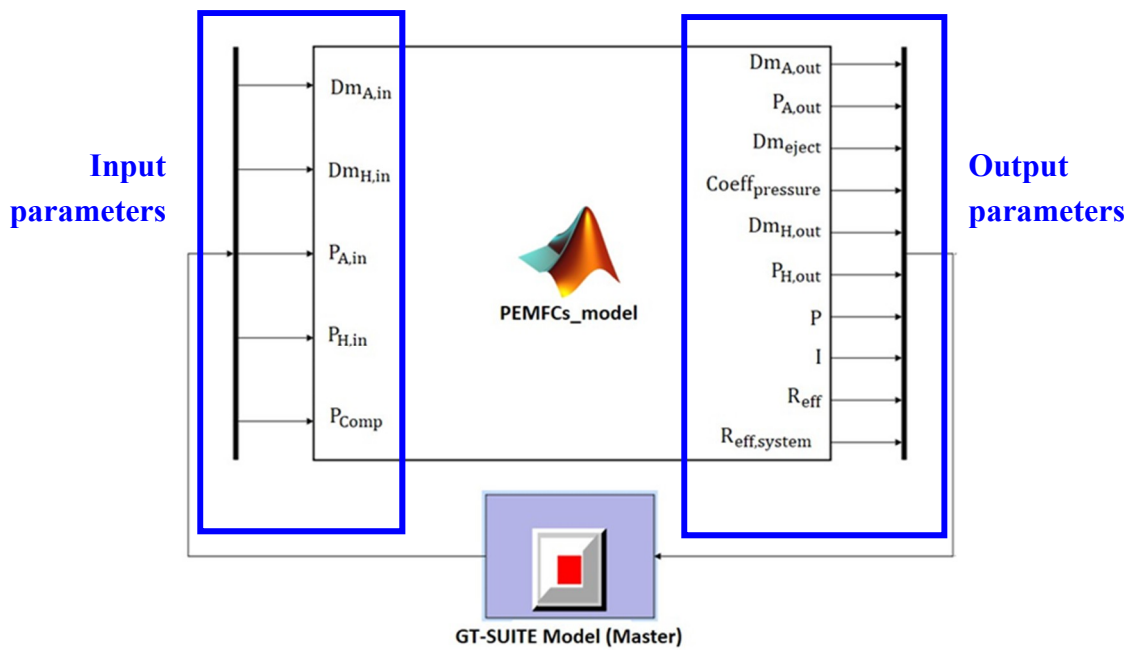


Figure 2. MATLAB/SIMULINK diagram using a Matlab function (PEMFCs_model) and a GT-SUITE master block.

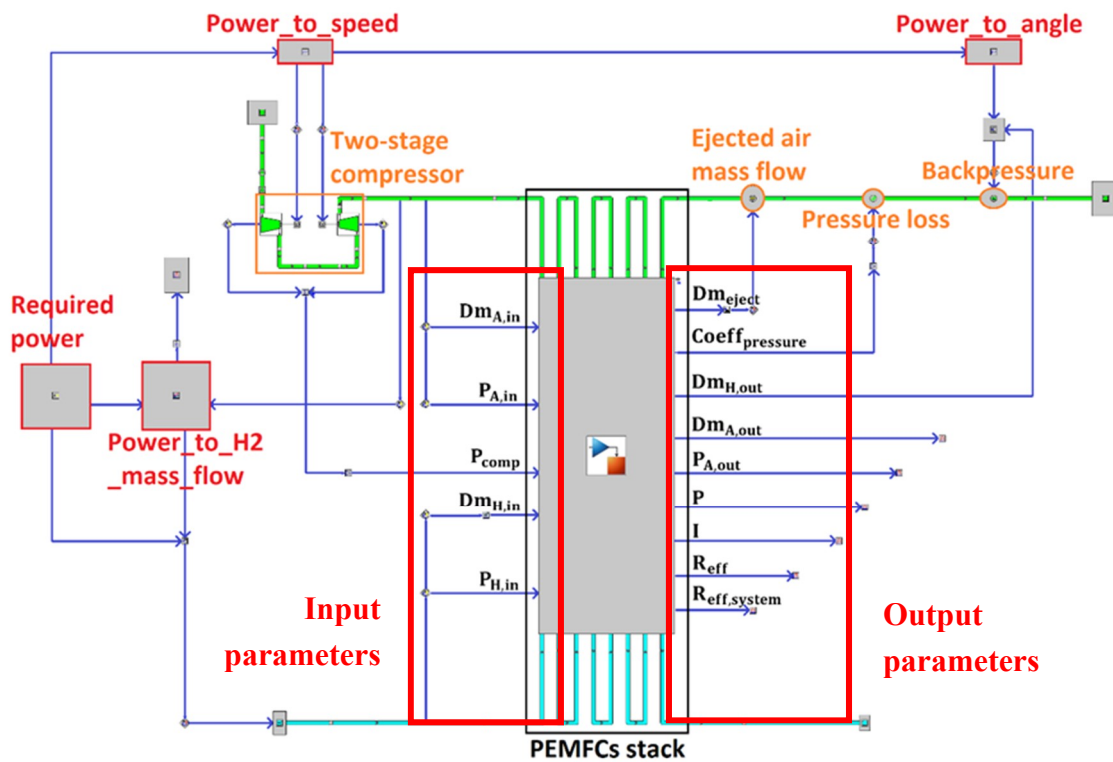


Figure 3. GT-SUITE diagram of a proton exchange membrane fuel cell (PEMFCs) stack model equipped with a two-stage electric compressor.

The potential advantages of a hybrid system are given as follows in Han et al. [9], Jeong [10] and Rodatz et al. [11] reducing the cost and weight of the global system; overcoming the relatively slow fuel cell system transient response; improving the hydrogen economy; and reducing the warm-up time of the fuel cell system to reach full power. Another significant advantage is the reduction of the physical constraints applied on the fuel cell, leading to an increase of the fuel cell stack system durability. Also, the degradation mechanism is still being investigated; it is possible to assure that the degradation of Pt catalysts is higher with high cell voltages Feroldi et al. [12].

2.2. Solid Oxide Fuel Cell (SOFC) Model

A polarisation curve model has been also used to model the operation of a monocell pure hydrogen solid oxide fuel cell (SOFC) with MATLAB/SIMULINK. The model used has been presented in a recent paper written by Zhu et al. [13]. This model takes into consideration the physical parameters of the cell such as diffusion coefficient and electrode thickness. It includes the Nerst potential, ohmic, activation, and mass transport losses, which are calculated as follows:

$$E_{\text{nerst}} = (1.253 - 0.000245 * T) + \frac{RT}{2F} \log \left(\frac{P'_{\text{H}_2} * P'^{0.5}_{\text{O}_2}}{P'_{\text{water}}} \right) \quad (14)$$

$$V_{\text{act}} = \frac{RT}{2F} \operatorname{arcsinh} \left(\frac{i}{2i_{0,\text{anode}}} \right) + \frac{RT}{2F} \operatorname{arcsinh} \left(\frac{i}{2i_{0,\text{cathode}}} \right) \quad (15)$$

where $i_{0,\text{anode}}$ and $i_{0,\text{cathode}}$ are the limiting current densities at the cathode and the anode, respectively. The mass transport losses are given by:

$$V_{\text{conc}} = -\frac{RT}{2F} \ln \left(\frac{P'_{\text{H}_2}}{P'_{\text{water}}} * \frac{P_{\text{W,in}}}{P_{\text{H,in}}} \right) - \frac{RT}{4F} \ln \left(\frac{P'_{\text{O}_2}}{P_{\text{O,in}}} \right) \quad (16)$$

where $P_{\text{H,in}}$, $P_{\text{W,in}}$ and $P_{\text{O,in}}$ are the stack inlet pressures of hydrogen, water, and oxygen, respectively. P'_{H_2} , P'_{water} and P'_{O_2} are the hydrogen, water, and oxygen pressures on the electrode's surface. They are given by the following equations:

$$P'_{\text{O}_2} = P_{\text{O,in}} - \left(\frac{i * RT}{P_{\text{A,in}} * 4F} \right) \left[(P_{\text{A,in}} - P_{\text{O,in}}) \left(\frac{l_{\text{c}(1)}}{D_{\text{O}_2-\text{N}_2}^{\text{eff}(1)}} + \frac{l_{\text{c}(2)}}{D_{\text{O}_2-\text{N}_2}^{\text{eff}(2)}} \right) \right] + \left(\frac{i * RT}{P_{\text{A,in}} * 4F} \right) \left[\frac{P_{\text{A,in}} - P_{\text{O,in}}}{P_{\text{A,in}}} \left(\frac{i * RT * l_{\text{c}(1)} * l_{\text{c}(2)}}{4F * D_{\text{O}_2-\text{N}_2}^{\text{eff}(1)} * D_{\text{O}_2-\text{N}_2}^{\text{eff}(2)}} \right) \right] \quad (17)$$

$$P'_{\text{H}_2} = \frac{l_{\text{a}(2)}}{D_{\text{H}_2-\text{H}_2\text{O}}^{\text{eff}(2)}} * \left[\frac{P_{\text{H,in}} * D_{\text{H}_2-\text{H}_2\text{O}}^{\text{eff}(2)}}{l_{\text{a}(2)}} - \left(\frac{i * RT * l_{\text{a}(1)}}{2F * D_{\text{H}_2-\text{H}_2\text{O}}^{\text{eff}(1)}} \right) \left(\frac{D_{\text{H}_2-\text{H}_2\text{O}}^{\text{eff}(2)}}{l_{\text{a}(2)}} + \frac{D_{\text{H}_2-\text{H}_2\text{O}}^{\text{eff}(1)}}{l_{\text{a}(1)}} \right) \right] \quad (18)$$

$$P'_{\text{water}} = \frac{l_{\text{a}(2)}}{D_{\text{H}_2-\text{H}_2\text{O}}^{\text{eff}(2)}} * \left[\frac{P_{\text{W,in}} * D_{\text{H}_2-\text{H}_2\text{O}}^{\text{eff}(2)}}{l_{\text{a}(2)}} + \left(\frac{i * RT * l_{\text{a}(1)}}{2F * D_{\text{H}_2-\text{H}_2\text{O}}^{\text{eff}(1)}} \right) \left(\frac{D_{\text{H}_2-\text{H}_2\text{O}}^{\text{eff}(2)}}{l_{\text{a}(2)}} + \frac{D_{\text{H}_2-\text{H}_2\text{O}}^{\text{eff}(1)}}{l_{\text{a}(1)}} \right) \right] \quad (19)$$

where $l_{\text{a}(1)}$ and $l_{\text{a}(2)}$ are the anode support and the anode functional layer thicknesses, respectively. The coefficients $l_{\text{c}(1)}$ and $l_{\text{c}(2)}$ are the cathode current collector and the cathode functional layer thicknesses, respectively. Concerning the diffusion coefficients, $D_{\text{H}_2-\text{H}_2\text{O}}^{\text{eff}(1)}$ and $D_{\text{H}_2-\text{H}_2\text{O}}^{\text{eff}(2)}$ are respectively the effective binary diffusivities through the anode support and the anode functional layer. $D_{\text{O}_2-\text{N}_2}^{\text{eff}(1)}$ and $D_{\text{O}_2-\text{N}_2}^{\text{eff}(2)}$ are respectively the effective binary diffusivities through the cathode current collector and the cathode functional layer. The ohmic losses are still given by Equation (8).

As seen in Figure 4, the MATLAB/SIMULINK model reiterated the principles of black box testing that were seen in the proton exchange membrane fuel cell (PEMFC) model. The efficiency R_{eff} was

still the electric efficiency of the stack, whereas the efficiency $R_{eff,GT}$ was the thermodynamic efficiency of the system {burner + gas turbine + heat exchanger}, which was calculated as follows:

$$R_{eff,GT} = \frac{P_{generator} + P_{heat}}{Dm_{A,in} * C_p * (T_{burner,out} - T_{burner,in})} \tag{20}$$

where C_p is the inlet burner air’s calorific capacity. $T_{burner,out}$ and $T_{burner,in}$ are the outlet and inlet burner temperatures, respectively, $P_{generator}$ is the electric power produced by the motor generator, and P_{heat} is the power transferred to the stack inlet air through the heat exchanger.

Many papers have referred to “system efficiency”. It must be noticed that $R_{eff,GT}$ is a thermodynamic efficiency, whereas R_{eff} is not. Nevertheless, it is possible to use a formulation as the ratio of the useful power and the theoretical maximum power. As a result, system efficiency can be formulated as follows:

$$R_{eff,system} = \frac{P + P_{generator} + P_{heat}}{(1.481 * N * I) + [Dm_{A,in} * C_p * (T_{burner,out} - T_{burner,in})]} \tag{21}$$

As seen in Figure 5, the GT-SUITE model of the hybrid system {SOFC + gas turbine} was similar to the PEMFC stack model. It must be noticed that this model included three proportional–integral–derivative (PID) controllers. The first one controlled the output power by taking into consideration the output power of the SOFC stack and the recovered power through the turbine. The second PID controlled the injection of the fuel into the burner. It adjusted the hydrogen mass flow rate to reach the targeted temperature. In an actual SOFC system, the hydrogen is not injected; rather, it is collected at the stack’s output [14]. Nevertheless, this model assumed a total consumption of the hydrogen at inlet. So, in order to consider the global consumption of hydrogen, an injector equipped with a controller was used. A classical burner output temperature for an SOFC stack using such a system is 1200 °C [14]. Finally, the target of 1130 °C was enough for the stack’s inlet temperature to reach more than 530 °C. The heat exchanger was based on the GT-SUITE example of a charge air cooler. Concerning PID 3, it controlled the pressure loss through the stack.

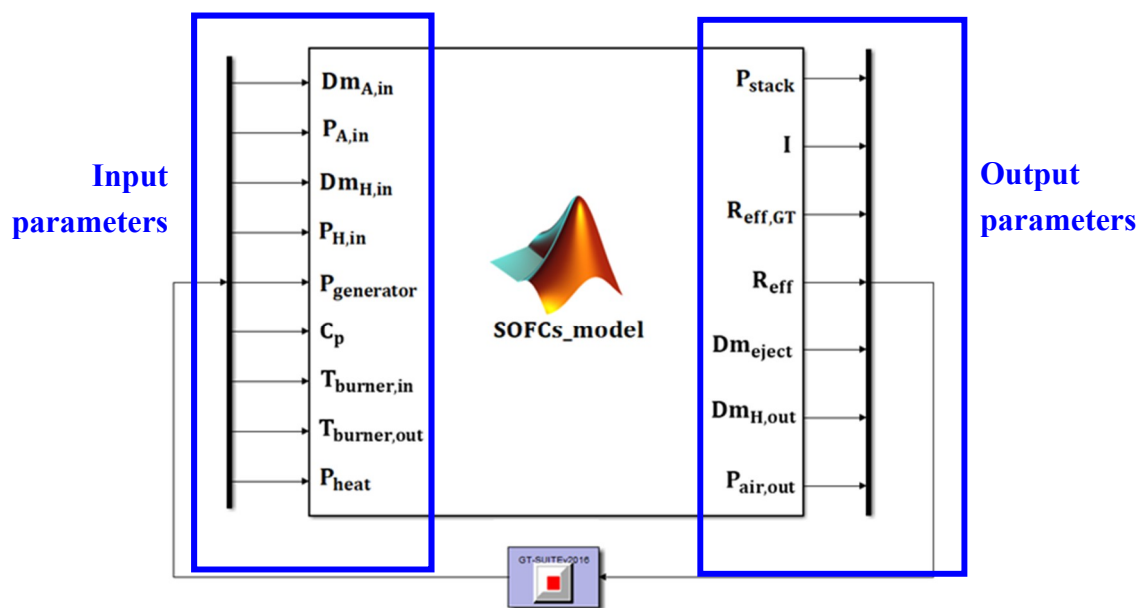


Figure 4. MATLAB/SIMULINK diagram of the 5 kW solid oxide fuel cells (SOFCs) stack.

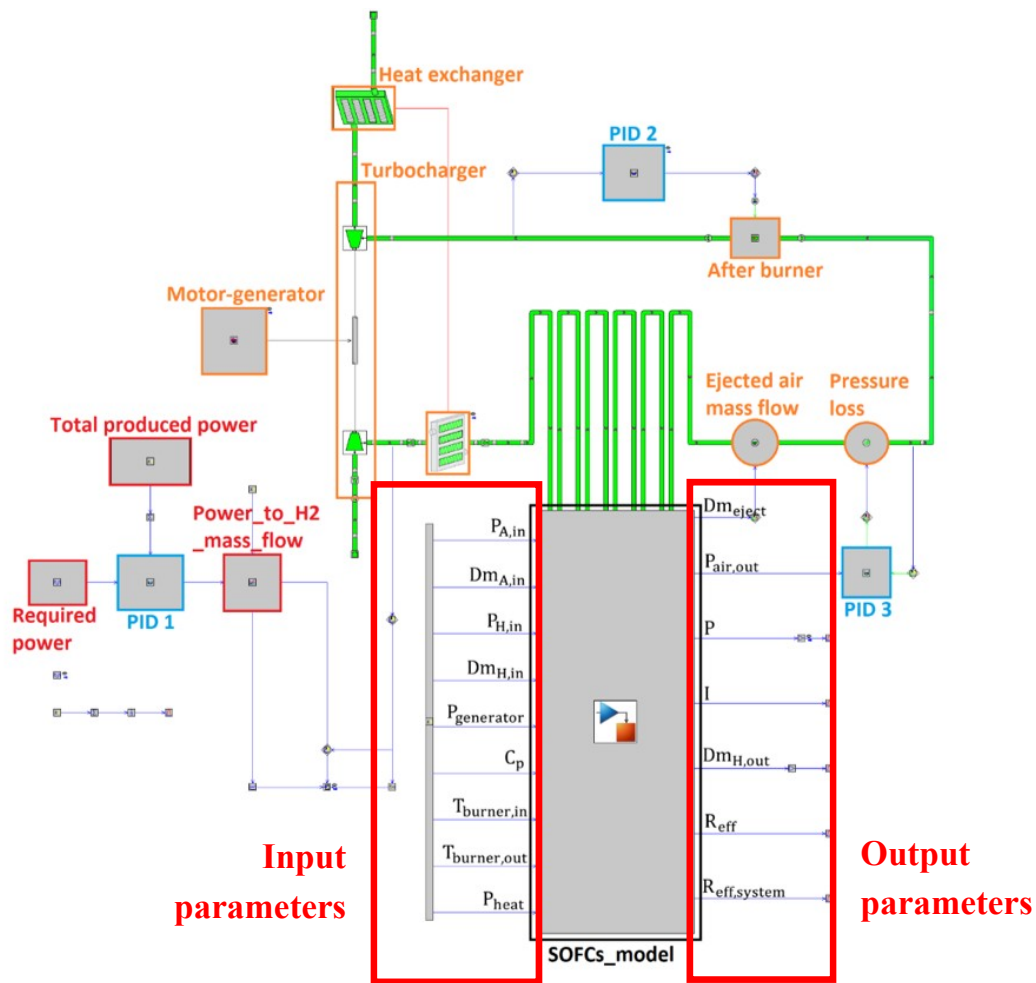


Figure 5. GT-SUITE model of the 5 kW SOFCs stack.

2.3. Compressor and Turbine Scaling Method

Air compressors must be adapted to the fuel cell application at hand and the requirements vary significantly compared to equivalent internal combustion engine systems. The compressors that were used in this study were derived from an Aeristech electric supercharger, which is able to reach a pressure ratio of 2.8 [15]. The experimental data that were used were adapted to this configuration by applying a reliable scaling method to adapt the compressor and the turbine to the size of the stack and the requirement of air mass flow [16–18].

2.4. Drive Cycle Simulation

Each PEMFC and SOFC powertrain has been optimised for the given required power. The optimisation included the adjustment of the backpressure, the hydrogen mass flow, the compressor speed, and the turbine geometry. The use of interpolation blocks of the optimised parameters enables proceeding to simulations of the Worldwide Harmonised Light Vehicle Test Procedure (WLTP) driving cycle. As seen in Figure 6, this 23.3-km driving cycle includes realistic urban and extra-urban driving conditions with credible acceleration and deceleration times.

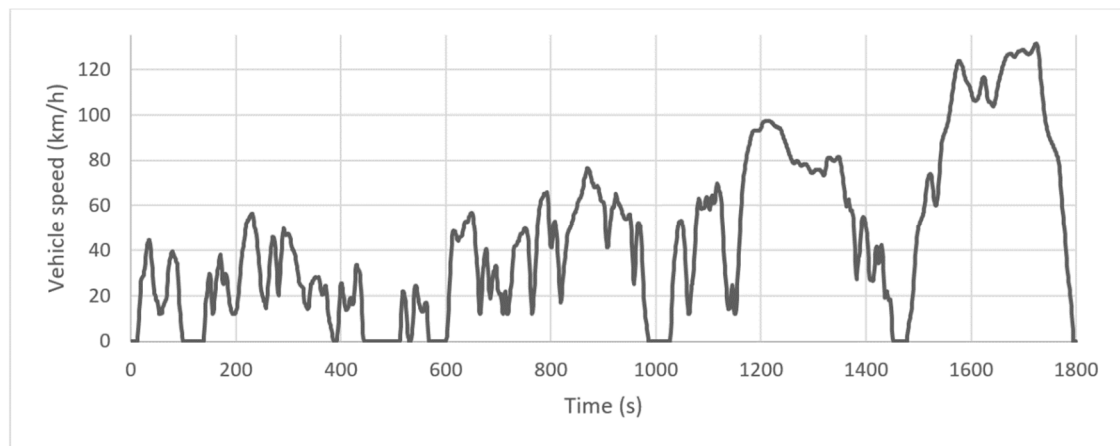


Figure 6. Vehicle speed through the Worldwide Harmonised Light Vehicle Test Procedure (WLTP) driving cycle.

3. Results

3.1. Types of Fuel Cells

Fuel cells can be classified according to the type of electrolyte that they employ. It determines the type of catalysis necessary, the operating temperature, and reactions into the cell such as steam reforming. Finally, fuel cells are classified as a function of the temperature at which the stack operates [19,20].

As seen in Table 1, a high operating temperature fuel cell does not require expensive catalysis such as platinum, and allows steam reforming (internal transformation of light fuels into hydrogen). The major issue with this type of cell is that quick starts are not allowed, which makes application to transportation impractical. To solve this problem, electrical resistances can be used, but this is a huge waste of energy. For instance, 4 Wh are necessary for a 200-W SOFCs stack to warm up from 20 °C to 700 °C in five minutes [21]. Nissan managed to build the first SOFC vehicle in 2016, using a 5 kW stack as an extender for the 24-kWh battery [22].

Low operating temperature fuel cells allow quick start, but they do not allow steam reforming, which limits the usable fuel type. Due to the high power density, low operating temperature condition, lower environmental impact than Phosphoric Acid Fuel Cell (PAFCs), and non-sensitivity to the CO₂ present in the air, the PEMFC is the most suitable fuel cell type for a transportation application. This includes personal and mass transit vehicles. As an example, Toyota sells the Sora, which is a fuel cell bus using two 114 kW PEMFC stacks of the same type as found on the Toyota Mirai fuel cell passenger car [23].

When PEMFCs are supplied with ethanol or methanol, the chemical reaction releases CO₂ as follows [24]:



Finally, pure hydrogen PEMFCs are more suitable than direct ethanol or methanol PEMFCs to comply with standards regarding CO₂ emissions, since the chemical reaction only releases water as follows:



Table 1. Fuel cell type classification [19,20];

Name of Fuel Cell		Solid Oxide Fuel Cell (SOFC)		Molten Carbonate Fuel Cell (MCFC)			
Electrolyte		Hard, non-porous ceramic		Molten carbonate salt mixture			
Operating Temperature		600–1100 °C		650 °C			
Fuel		Pure hydrogen, biogas or light fossil fuel		Hydrocarbon fuels			
High operating temperature fuel cell	Benefits	<ul style="list-style-type: none"> • Non-precious metal for catalysis • Able to reform methanol and ethanol • Mechanically simple: it is a solid-state device. • Vehicle auxiliary power units, medium to large scale power generation and Combined Heat and Power (CHP), off-grid power and micro CHP. 		<ul style="list-style-type: none"> • Non-precious metal for catalysis • Efficiency: from 50% to 85% with cogeneration • No carbon monoxide or dioxide poisoning 			
	Drawbacks	<ul style="list-style-type: none"> • High operating temperature • Complexity of heat management • The ceramic materials used are expensive to manufacture, and are also fragile. 		<ul style="list-style-type: none"> • High operating temperature • Poisoning by sulphur • Use hydrocarbon fuel = greenhouse gas emissions 			
Name of Fuel Cell		Proton Exchange Membrane Fuel Cell (PEMFC)		Alkaline Fuel Cells (AFCs)		Phosphoric Acid Fuel Cell (PAFCs)	
Electrolyte		Solid polymer (acid membrane)		Polymer (alkaline membrane)		Liquid phosphoric acid	
Operating Temperature		80–100 °C		100–250 °C		250–300 °C	
Fuel		Pure hydrogen or methanol/ethanol (direct or indirect)		Pure hydrogen, borohydride, or zinc		Hydrocarbon fuel	
Low operating temperature fuel cell	Benefits	<ul style="list-style-type: none"> • Low operating temperature • Quick start • Environmentally friendly • High power density 	<ul style="list-style-type: none"> • High efficiency (60%) • Non precious metal for catalysis 		<ul style="list-style-type: none"> • High power (over 75 MW) • High overall efficiency (80%) when combined with cogeneration 		
	Drawbacks	<ul style="list-style-type: none"> • Use platinum for the catalysis • Sensitive to carbon monoxide • Water management 	<ul style="list-style-type: none"> • Sensitive to carbon dioxide (the percentage in the air is enough to destroy the cell) 		<ul style="list-style-type: none"> • Greenhouse gas emissions • Low efficiency without cogeneration (less than 40%) 		

The high operating temperature of a SOFC allows the internal reforming of light fuels into hydrogen, but it produces CO₂. In the case of pure hydrogen as fuel, even if the chemical reactions at the cathode and the anode are different than the PEMFC's ones, the global reaction is the same as that of Equation (23). Nevertheless, the compactness of a SOFC stack is far lower than that of a PEMFC. For instance, the SteelCell[®], developed by CeresPower to extend the driving range of an electric vehicle, reaches 500 W/L, which is six times less than the new Toyota Mirai's stack [25,26]. The 1 kW CeresPower stack weight is 9.3 kg (107 W/kg) [27] which means that, for the same output power, a SOFC stack is almost 19 times heavier than the PEMFC one, which reaches 2 kW/kg. As a result, SOFC technology seems to be only relevant for use as a range extender.

3.2. Boosting Options for PEMFCs

Similarly to Internal Combustion Engines (ICEs) using boosting systems (air compressors (superchargers) or turbochargers) to increase their power density and efficiency, a boosting system can be used with a fuel cell stack to increase its performance. However, the requirements are not the same. Firstly, an air compressor for fuel cells needs a high pressure with a low air mass flow rate. Secondly, because of the battery, the stack, the control power unit, and the hydrogen storage tanks, the size of the boosting system needs to be considered in a transportation application. In most ICE applications, a turbocharger is used to recover the energy from high-temperature exhaust gas. Even if an expander is used, the operating temperature of the PEMFC (80 °C) is too low to recover enough power to drive the compressor. It implies that the air supply system uses power from the stack. As a consequence, a high efficiency is an important requirement.

As seen in Table 2, centrifugal and Roots compressors are the most suitable for fuel cell application [28–32]. They are smaller and cheaper than screw and scroll compressors, and help to reduce the weight and the cost of PEMFCs vehicle, which is already increased by the use of platinum.

Daimler, General Motor, and SAIC as an example use centrifugal compressors, as part of their electric-assisted turbochargers (E-turbochargers) [28]. The Honda FCX Clarity uses a screw compressor, but the new Honda Clarity fuel cell is now equipped with a two-stage centrifugal compressor, which has a 50% smaller sound absorber than the FCX screw compressor [4]. Toyota remains the only FCV manufacturer to use a Roots compressor. This type of compressor has a lower efficiency and pressure ratio, but higher power density than the centrifugal compressor. However, the pulsation noise implies the use of a bigger sound absorber. As a result, FCV manufacturers have adopted centrifugal compressors as the most suitable compressor type for fuel cell applications.

Two-stage compressors and E-turbochargers are currently used for FCV applications. The Honda Clarity fuel cell two-stage compressor reaches a 4:1 pressure ratio [4]. An estimated pressure ratio value of 2.8:1 is given by a recent paper for an E-turbocharger [33]. Figure A1 in the Appendices provides an illustration of this two-stage system. This paper also proposed a mixed architecture with a two-stage compressor and a turbine generator to reduce the energy consumption of the boosting system.





3.3. Boosting Options for SOFCs

The most promising boosting option for SOFC application is a compressor coupled to a E-turbocharger in order to recover the wasted energy [10,34,35].

Many different architectures can be considered to build a hybrid system between a SOFC stack and an E-turbocharger. As seen in Figure 7, the SOFC stack can be placed before the turbine [36]. As a result, the air pressure into the stack is higher than the ambient pressure. This type of architecture is called a pressurised cycle. Some systems, which are called atmospheric cycles, place the stack after the turbine [37], forcing the SOFC stack to operate at ambient pressure. The atmospheric cycle is simpler and more reliable than the pressurised one. However, given that the efficiency of the SOFC increases with pressure, it is expected to achieve less electric efficiency than the pressurised configuration. Plus, the latter is also cheaper, since it needs fewer components [38]. As a result, the choice of the architecture

depends on the application requirements. For a high electric efficiency system, the pressurised cycle must be chosen, whereas the atmospheric cycle may be used for its reliability.

Table 2. Comparison of centrifugal, roots, screw, and scroll compressors [24–28]. ★: very bad; ★★: bad; ★★★: good; ★★★★: very good; ★★★★★: excellent.

Type of Compressors	 Centrifugal	 Roots	 Screw	 Scroll
Compactness	★★★★★	★★★★	★	★
Weight	★★★★	★★★★	★★	★★
Temperature rise	★★★	★	★★★★★	★★★★
Pulsations, noise	★★★★	★★	★★★	★★★★
Compression	★★★	★★★★	★★★★★	★★★★★
Cost	★★★★	★★★★★	★★	★★
Durability	★★★	★★★★★	★★★	★★★★
Average rating	3.7/5	3.0/5	2.7/5	2.6/5

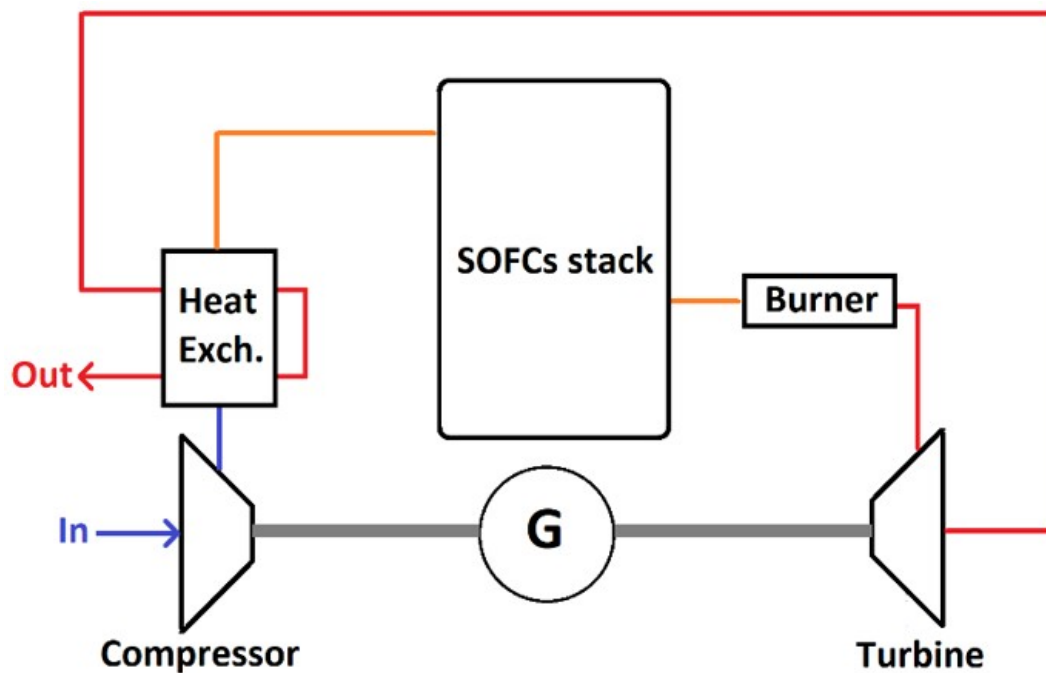


Figure 7. Example of a pressurised air supply system for an solid oxide fuel cell (SOFC) stack.

3.4. PEMFC Powertrain Simulation

To compare air supply systems, two different PEMFC stacks have been considered. Both have a 350 cm² active area and reach a 78 kW maximum output power. The first one is a 360-cell stack equipped with either an E-turbocharger or a single-stage compressor. The second one is a 315-cell stack equipped with a two-stage compressor. As a result, vehicles equipped with the 315-cell stack weigh 1850 kg, whereas the 360-cell stack vehicles have a five-kg excess weight [39].

The stack provides the entire power to propel the car and drive the air supply system. In each case, the air supply system has been optimised to reach the highest system electric efficiency, and thus it has the highest driving range with a 5.6-kg hydrogen storage tank [40]. Both stacks operate with a constant 3 bar pressure for the hydrogen supply system and operate at 80 °C. The overall model layout of the FCV is provided in Figure A3 in the appendices.

The same compressor has been used for configurations 1 and 2. Only the performance map has been adapted for each configuration. The map is provided in the appendices (Figure A2). The single-stage compressor uses a backpressure, whereas the E-turbocharger has a turbine at the stack outlet. As seen in Table 3, the E-turbocharger system reaches a higher system electric efficiency average, and thus a 3.5% higher driving range. Due to the turbine, the average power that is required to drive the compressor in the E-turbocharger is 46% lower than the required average power for the single-stage compressor. During the maximum acceleration phase, the turbine recovers 2.4 kW, and thus required a relative power difference of 20%.

Table 3. Results of the WLTP driving cycle simulation.

Configuration number	1	2	3
Number of cells		360	315
Air supply system	E-turbocharger	Single-stage compressor	Two-stage compressor
Pressure range (bar)	[1.1–2.3]	[1.1–2.2]	[1.1–2.7]
Average system electric efficiency (%)	32.1	28.8	30.5
Average stack electric efficiency (%)	61.7	61.6	61.2
Average compressor/turbine efficiency (%)	76.8/51.6	77.9/–	60.2/–
Driving range (km) for 5.6 kg of hydrogen	706	682	681

By reducing the number of cells, the mass transfer losses increase, since it is harder for reactants to reach the catalysis area. As seen in Figure 8, the stack electric efficiency decreases. The two-stage compressor has been designed to reach 4.0 bar. During the WLTP driving cycle, the two-stage compressor average pressure is 4.9% higher than the E-turbocharger one, which could have compensated for the increase of mass transfer losses. However, the average power required for the two-stage compressor is 43% higher than the power required for the E-turbocharger. This leads to a 1.6% absolute change in the lower system electric efficiency average, and a 3.5% lower driving range than the E-turbocharger configuration.

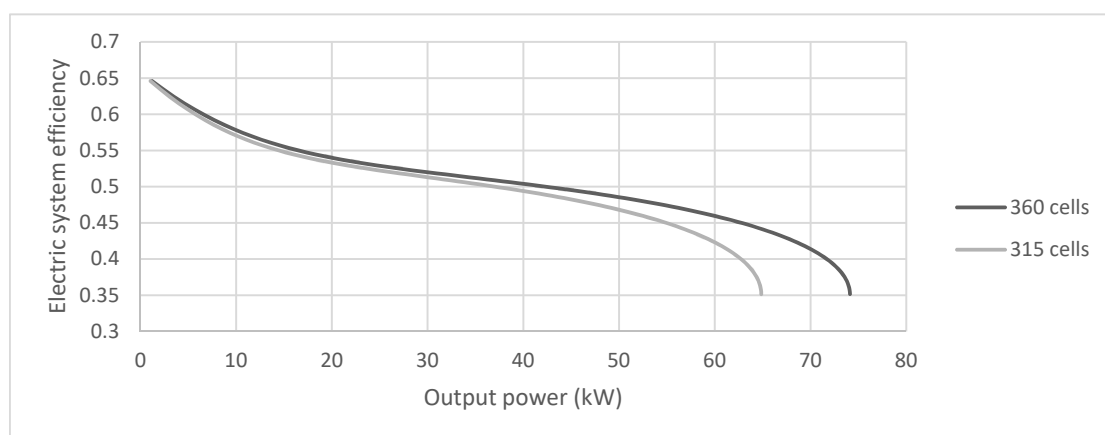


Figure 8. Impact of the number of cells on the stack electric efficiency (operating at two bar).

As seen in Figure 9, the model used for the PEMFC underestimated the output power when the operating pressure was between 1.0–1.7 bar, with an overestimation above this value. However, the results of the comparison between the different air supply systems were valid, even if the influence of the operating pressure was underestimated or overestimated.

The single-stage compressor map outcome is provided in the appendices, in Figures A4 and A5.

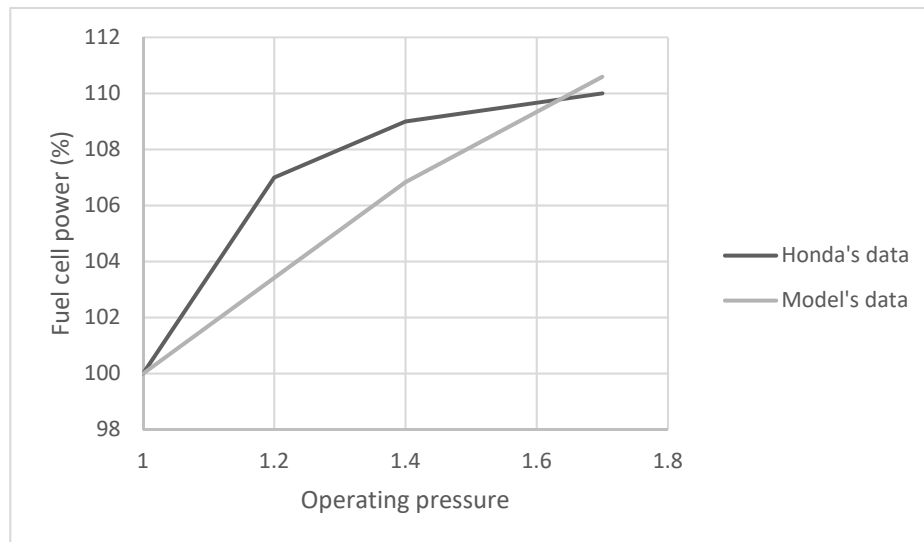


Figure 9. Comparison between Honda's data and the model's data of the operating pressure influence on the output power.

3.5. SOFC Powertrain Simulation

The purpose of this part was to study an electric vehicle using the SOFC technology as a range extender, based on the Nissan e-NV200 van equipped with a 5 kW SOFC stack.

The SOFC model was a 5 kW stack using pure hydrogen as fuel. The internal ohmic resistance in the polarisation curve model has been adapted to match the power density of a metal-supported SOFC operating at 550 °C that was found in the literature. Since the stack reached only 5 kW, the required air mass flow rate was very low. As a result, the compressor that was used in this model was derived from the Aeristech electric supercharger by reducing the compressor and the turbine wheels diameters. The motor-generator model was based on a literature review of a high-speed motor generator for a microturbine [41,42]. The electric version of the Nissan EV-200N weighed 1685 kg [38], while the vehicle used for the simulations weighed 1740 kg.

Concerning the fuel cell system, when it operated at 5 kW, the system efficiency $R_{(eff,system)}$ reached 67%. The SOFCs stack provided 4.6 kW, and the generator produced 0.4 kW. As seen in Figure 10, the inlet air mass flow was $15.7 \text{ g}\cdot\text{s}^{-1}$ under 1.48 bar. The total hydrogen mass flow rate was $0.159 \text{ g}\cdot\text{s}^{-1}$, of which 39% was used in the SOFC stack under 3 bar, and 61% was released into the burner to increase the turbine inlet temperature to 1130 °C.

Simulations were conducted through the WLTP driving cycle (described by Figure 6) for an increase in the initial state of charge (SOC) from 10% to 90%. The driving calculation was based on the Nissan SOFC vehicle specifications: the ethanol tank capacity is 30 litres [38]. With a density of 0.789, the ethanol was transformed into 6.2 kg of hydrogen.

The first power management strategy tried to find a compromise between hydrogen consumption and driving range. When the operating SOC was between 0–60%, the range extender output power was 3 kW in order to maximise the driving range. From 60% to 80%, the output power was 3 kW; then, the range extender was turned off above 90% to reduce the hydrogen consumption.

As seen in Figure 11, a vehicle equipped with the range extender, a hydrogen tank capacity of 6.2 kg, and an initial SOC of 100%, reached 590 km. This was 236% higher than the pure electric vehicle (driving range for an initial SOC of 100%: 178 km). It must be noticed that when the power management strategy was n°1, 551 km was driven before the hydrogen tank emptied.

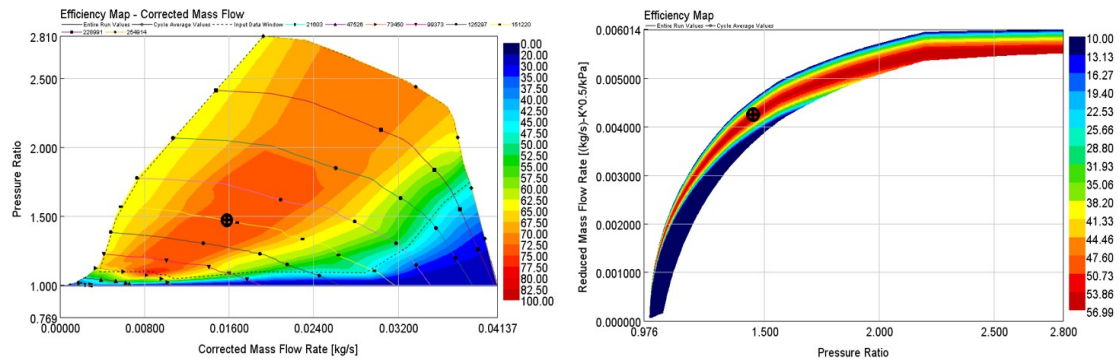


Figure 10. Operating points on the compressor (left) and turbine maps (right) when the SOFC system operated at 5 kW.

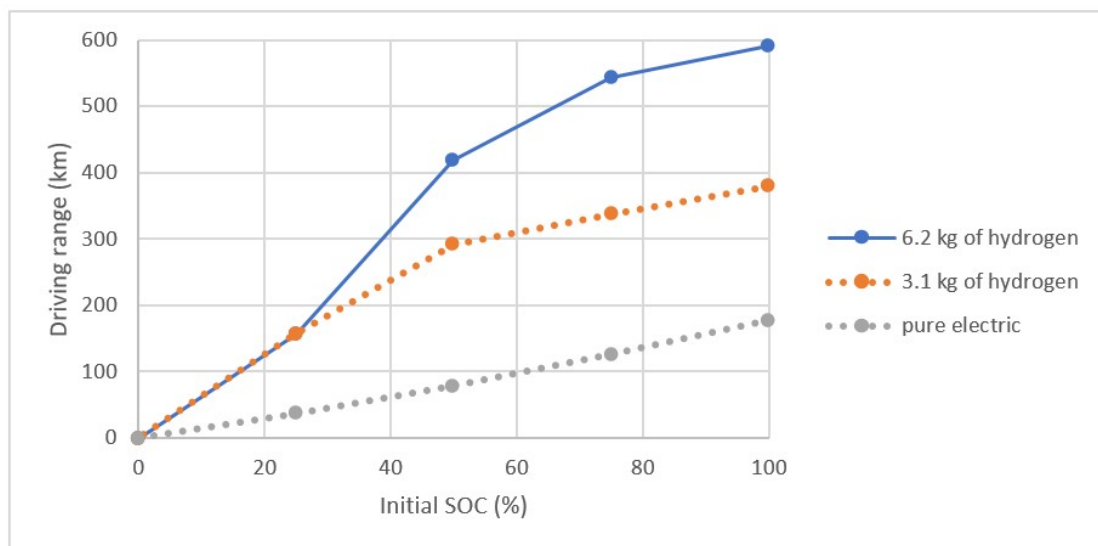


Figure 11. Calculated driving range for different initial SOC and tank capacities.

With half of the hydrogen tank’s capacity and an initial SOC of 100%, the driving range reached 379 km, which was 113% higher than the pure electric vehicle driving range.

It was possible to increase the driving range per tank of hydrogen by recharging the vehicle when the SOC was under 60%. With five charge cycles from 60% to 100% every 156 km, the vehicle reached 759 km with only one full tank of hydrogen.

Then, it was also possible to increase the driving range with only one charge cycle by using the maximum output power of the range extender all of the time. Previously, the power unit control reduced the power of the range extender from 5 kW to 3 kW when the SOC exceeded the limit of 60% in order to reduce the hydrogen consumption. By keeping the output power at 5 kW enabled the reduction of Δ SOC per kilometre. As a result, the driving range was increased by 6.1% compared to the original power management strategy, to reach 626 km. Nevertheless, the driving range per tank of hydrogen decreased by 9.1%, to reach 501 km.

According to a Nissan report [43], the driving range of their solid oxide fuel cell vehicle using a 5 kW range extender was 600 km. So, the previous simulations results matched with the Nissan vehicle's specification well.

Since the driving range depends on the initial SOC and amount of hydrogen, two strategies can be used: optimising the driving range of the vehicle per tank of fuel (strategy n°1) or per charge cycle (strategy n°2). In addition, this also depends on the frequency at which the battery is charged. There is also an aspect of electric vehicles that cannot be ignored: to conserve the battery as long as possible, the best range of usable SOC is 40% to 70%. During the first discharge cycle from 70% to 40%, the first strategy of power management led to a driving range of 327 km. As a result, 37% of the usable hydrogen remained. During the second discharge cycle from 70% to 40%, the driving range was 211 km (of which 193 km were achieved with the range extender mode). This led to a global driving range of 538 km after two charge cycles from 40% to 70%.

4. Conclusions

The literature review and the co-simulations between MATLAB/SIMULINK and GT-SUITE underlined that two types of fuel cells are really promising for transportation application: the PEMFC and the SOFC.

The first one is a fuel cell operating at 80 °C, which allows a fast and simple start-up. Nevertheless, in this operating condition, the compressor must be powered by the stack, which decreased the useful power transmitted to the wheels. The use of a turbine, coupled with the compressor, reduced the power that the air supply system required by 45.8%, on average. As a result, the driving range of the vehicle increased by 3.5% and reached 706 km with an average electric efficiency of 32.1%. This was 11.5% better than the single-stage configuration's electric efficiency. However, to deal with the compactness of the PEMFC stack, the two-stage compressor emerged as a real asset. By increasing the maximum pressure ratio from 2.8 bar to 4.0 bar, it decreased the number of cells that were necessary to reach the same output power by 12.5%. Unfortunately, this downsizing operation had an impact on voltage losses. Finally, the two-stage compressor reached a similar driving range to the single-stage configuration. It can be interesting to compare these results with a roots compressor, such as the one used by Toyota for their FCVs.

The second one is a fuel cell operating between 550–1000 °C. The low power density (about 9.3 kg·kW⁻¹) and the impossibility of a quick start-up make the use of this technology as a pure propulsion system irrelevant at the moment. Nevertheless, the high operating temperature allows combining a SOFC stack and a gas turbine together into a hybrid system. The use of this technology as a range extender for an electric vehicle is truly promising. It allows extending the driving range by 252%. The driving range, with an initial SOC of 100% and a 6.2-kg tank full of pure hydrogen, reached more than 600 kilometres. It must be noticed that this result depended on the power management strategy. With an optimisation of the driving range per charge cycle, the vehicle reached 626 kilometres. A different strategy can also be used to optimise the driving range per tank of hydrogen. In this case, it reached 759 km due to five charge cycles from 60% to 100%.

The use of PEMFC and SOFC technologies are fundamentally different. The first is used as a propulsion system, whereas the second is used as a range extender. The development and the optimisation of the latter is more complex in term of power management. Plus, the driving range really depends on the driver's behaviour on the road and the frequency at which the battery is charged. In 2015, the kWh European average price was 0.205 € [44]. In 2017, the kilogram of hydrogen price was 15 € in an Air Liquide station [45]. As a result, the first strategy of power management described in the previous paragraph leads to a price of 0.166€ per kilometre for a SOFC/electric hybrid vehicle, whereas the optimised driving range per tank of hydrogen leads to 0.135 € per kilometre. For a PEMFC vehicle using an E-turbocharger, the price per kilometre is 0.119 €. This difference is partially due to the consumed hydrogen into the burner to warm the inlet air through the heat exchanger. As a result, it could be interesting to evaluate the performances of a vehicle using a PEMFC stack as a

range extender instead of a SOFC one. This result matches with most of the fuel cell vehicles using the PEMFC technology, which is simpler and cheaper to use. However, this result must be nuanced, since the production of hydrogen is not as developed as power generation, which explains the high price of the fuel.

Author Contributions: A.K. was the student who carried out the modelling effort at Brunel University London and his work was checked by A.M., also a research student at Brunel, who also drafted the paper. A.P., is the turbomachinery group leader in the Centre of Advanced Powertrains and Fuels (CAPF) at Brunel University London, who conceived of the project, the layout of the investigations and checked the computational outcome of the resultant modelling effort and subsequent discussion. In this he was assisted by D.C., who was A.K.'s supervisor at his home institution of Ecole Centrale de Nantes.

Funding: This research received no external funding.

Conflicts of Interest: The authors declare no conflict of interest.

Nomenclature

CHP	Combined Heat and Power
Coeff _{pressure}	Pressure loss coefficient
C_p	Inlet burner air specific heat capacity
$D_{H_2-H_2O}^{eff(1)}$	Effective binary diffusivity through the anode support
$D_{H_2-H_2O}^{eff(2)}$	Effective binary diffusivity through the anode functional layer
$D_{O_2-N_2}^{eff(1)}$	Effective binary diffusivity through the cathode current collector
$D_{O_2-N_2}^{eff(2)}$	Effective binary diffusivity through the cathode functional layer
$Dm_{A,in}$	Inlet air mass flow
$Dm_{A,out}$	Outlet air mass flow
Dm_{eject}	Ejected air mass flow
$Dm_{H,in}$	Inlet hydrogen mass flow
$Dm_{H,out}$	Outlet hydrogen mass flow
$Dm_{O,in}$	Inlet oxygen mass flow
$Dm_{O,out}$	Outlet oxygen mass flow
E_{Nerst}	Nerst potential
F	Faraday constant
FCV	Fuel cell vehicle
I	Current
ICE	Internal combustion engine
i	Current density
$i_{0,anode}$	Anode limiting current density
$i_{0,cathode}$	Cathode limiting current density
i_L	Limiting current density
$l_{a(1)}$	Anode support thickness
$l_{a(2)}$	Anode functional layer thickness
$l_{c(1)}$	Cathode current collector thickness
$l_{c(2)}$	Cathode functional layer thickness
M_H	Hydrogen molar mass
N	Number of cells
P	Stack output power
$P_{A,in}$	Inlet air pressure
$P_{A,out}$	Outlet air pressure
P_{comp}	Compressor required power
$P_{generator}$	Produced power by the generator
$P_{H,in}$	Inlet hydrogen pressure
P_{H2}	Average hydrogen pressure
P'_{H2}	Hydrogen pressure on the electrolyte surface

P_{heat}	Heat power exchanged
PEMFC	Proton exchange membrane fuel cell
PID	Proportional–integral–derivative
$P_{O,in}$	Inlet oxygen pressure
P_{O2}	Average oxygen pressure
P'_{O2}	Oxygen pressure on the electrolyte surface
P_{sat}	Water saturation pressure
$P_{W,in}$	Inlet water pressure
P'_{water}	Water pressure on the electrolyte surface
R	Gas constant
R_{eff}	Stack electric efficiency
$R_{eff, GT}$	Gas turbine efficiency
$R_{eff,system}$	System efficiency
R_i	Internal cell resistance
SOC	State of charge
SOFC	Solid oxide fuel cell
T	Operating temperature
$T_{burner,in}$	Inlet burner temperature
$T_{burner,out}$	Outlet burner temperature
V	Voltage
V_{act}	Activation losses
V_{conc}	Mass transport losses
V_{losses}	Voltage losses
V_{ohm}	Ohmic losses
WLTP	Worldwide harmonised light vehicle test procedure

Appendix A

Two-Stage Compressor

Two-stage supercharging

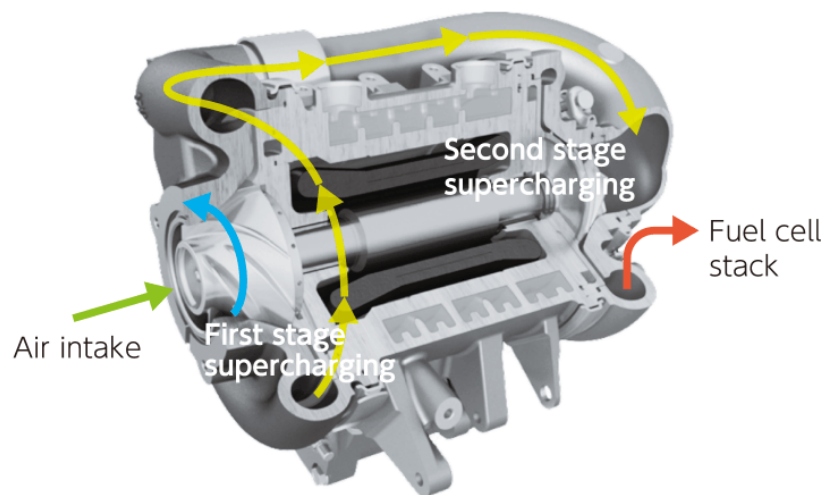


Figure A1. Two-stage compressor used in the Honda Clarity Fuel Cell.

E-turbocharger

To model this type of air supply system, a conventional turbocharger coupled with an additional input shaft power control module (to replicate the electric motor) was used as seen in Figure A2. The turbine was a Variable Nozzle Geometry (VNT) type.

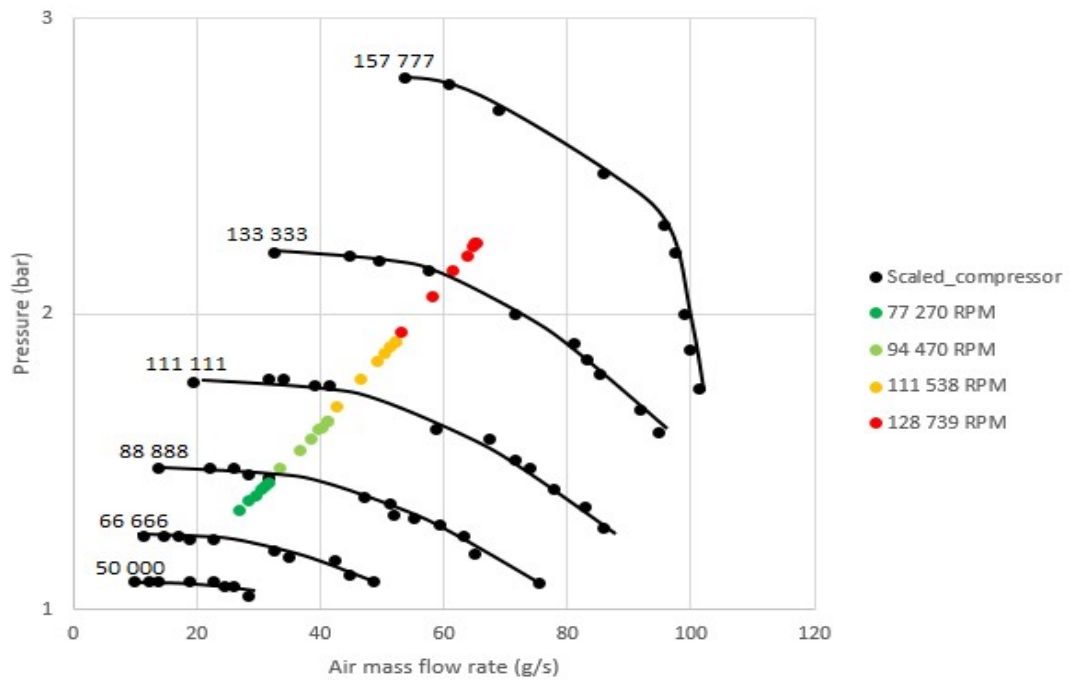


Figure A2. Compressor and turbine rack 0.4 maps of the E-turbocharger.

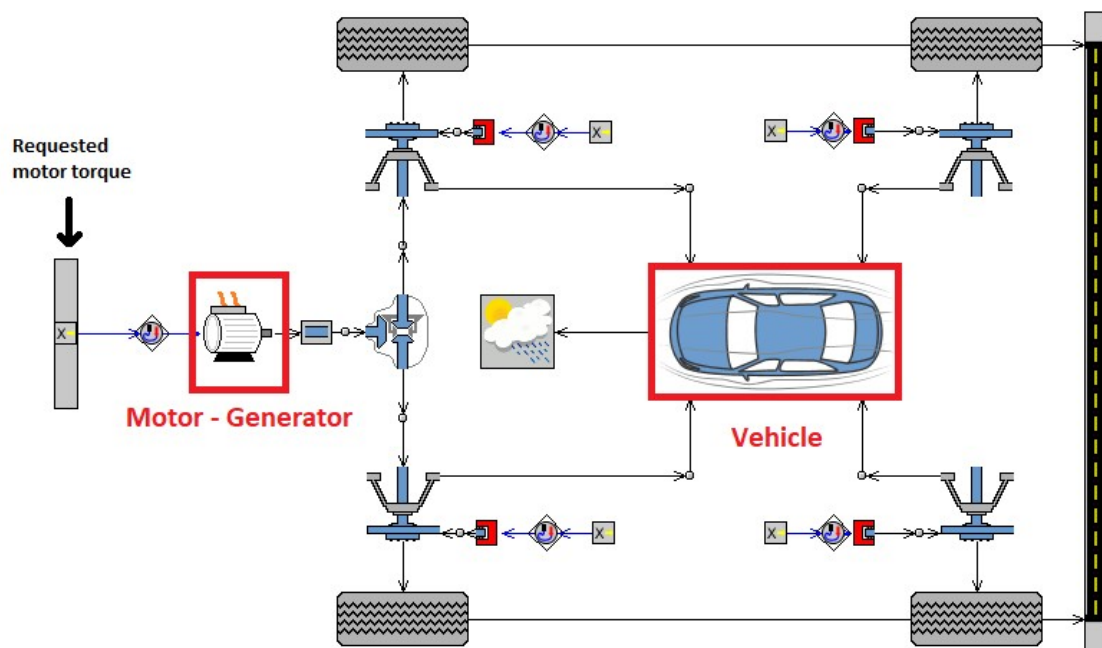


Figure A3. GT-SUITE diagram of the powertrain—vehicle frame and motor—generator.

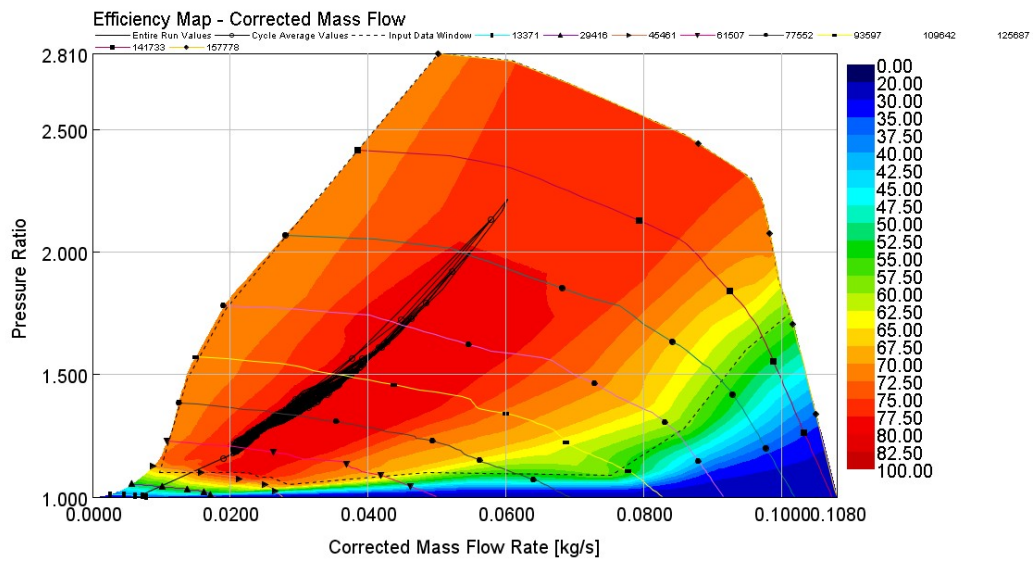


Figure A4. Single stage compressor map for PEMFC application.

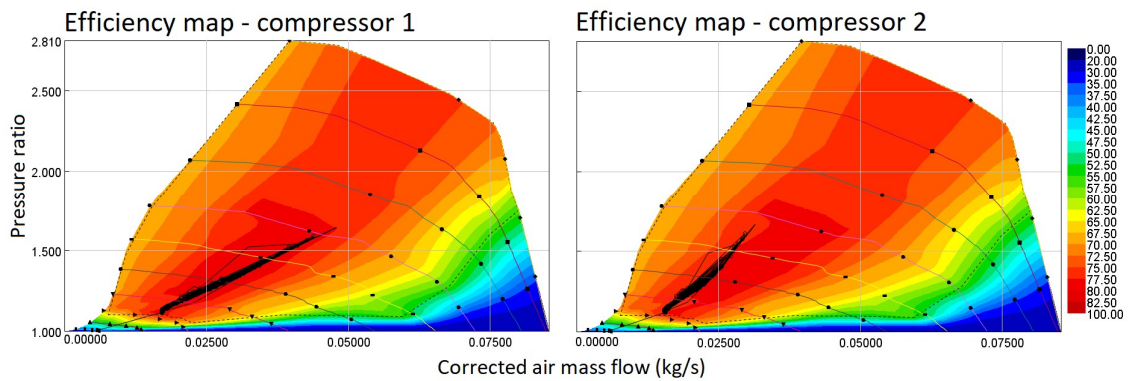


Figure A5. Efficiency map of two-stage centrifugal compressors for PEMFC application.

References

- Edenhofer, O.; Pichs-Madruga, R.; Sokona, Y.; Minx, J.C.; Farahani, E.; Kadner, S.; Seyboth, K.; Adler, A.; Baum, I.; Brunner, S.; Erikemeier, P.; et al. *Climate Change 2014: Mitigation of Climate Change; Contribution to the Fifth Assessment Report of the Intergovernmental Panel on Climate Change*; Cambridge University Press: Cambridge, UK, 2014.
- The Union of Concerned Scientists. *How Clean Are Hydrogen Fuel Cell Electric Vehicles?* The Union of Concerned Scientists: Cambridge, MA, USA, 2014.
- Andwari, A.M.; Pesiridis, A.; Rajoo, S.; Martinez-Botas, R.; Esfahanian, V. A review of Battery Electric Vehicle technology and readiness levels. *Renew. Sustain. Energy Rev.* **2017**, *78*, 414–430. [CrossRef]
- Sugawara, T.; Kanazawa, T.; Imai, N.; Tachibana, Y. *Development of Motorized Turbo Compressor for Clarity Fuel Cell*; SAE International: Warrendale, PA, USA, 2017.
- Pukrushpan, J.T.; Stefanopoulou, A.G.; Peng, H. *Control of Fuel Cell Power Systems: Principles, Modeling, Analysis and Feedback Design*; Springer: Berlin, Germany, 2004; ISBN 1-85233-816-4.
- Cruz Rojas, A.; Lopez Lopez, G.; Gomez-Aguilar, J.F.; Alvarado, V.M. Cinda Luz Sandoval Torres. Control of the air supply subsystem in a PEMFC with balance of plant simulation. *Sustainability* **2017**, *9*, 73. [CrossRef]
- Fuel Cell Formulary. Available online: http://www.pemfc.de/FCF_A4.pdf (accessed on 21 May 2018).
- Candusso, D. *Hybridation du Groupe Électrogène à Pile à Combustible pour L'alimentation d'un Véhicule Électrique. Energie Électrique*; Institut National Polytechnique de Grenoble—INPG: Grenoble, France, 2002.
- Han, J.; Kokkolaras, M.; Papalambros, P.Y. Optimal design of hybrid fuel cell vehicles. *ASME. J. Fuel Cell Sci. Technol.* **2008**, *5*, 041014. [CrossRef]

10. Jeong, K.S.; Oh, B.S. Fuel economic and life-cycle cost analysis of a fuel cell hybrid vehicle. *J. Power Sources* **2002**, *105*, 58–65. [CrossRef]
11. Rodatz, P.; Paganelli, G.; Sciarretta, A.; Guzzella, L. Optimal power management of an experimental fuel cell/supercapacitors-powered hybrid vehicle. *Control Eng. Practice* **2004**, *13*, 41–53. [CrossRef]
12. Feroldi, D.; Serra, M.; Riera, J. Design and analysis of fuel-cell hybrid systems oriented to automotive applications. *IEEE Trans. Veh. Technol.* **2009**, *58*, 4720. [CrossRef]
13. Zhu, L.; Zhang, L.; Virkar, A.V. A parametric model for solid oxide fuel cells based on measurements made on cell materials and component. *J. Power Sources* **2015**, *291*, 138–155. [CrossRef]
14. Azizi, M.A.; Brouwer, J. Progress in solid oxide fuel cell-gas turbine hybrid power systems: System design and analysis, transient operation, controls and optimization. *Appl. Energy* **2018**, *215*, 237–289. [CrossRef]
15. Electric Supercharger Map, Aeristech. Available online: <http://www.aeristech.co.uk/electric-supercharger/> (accessed on 20 April 2018).
16. Ernst, B.; Kammeyer, J.; Seume, J.R. Improved map scaling methods for small turbocharger compressors. In Proceedings of the Improved map scaling methods for small turbocharger compressors, Vancouver, BC, Canada, 6–10 June 2011.
17. Schleer, M.; Abhari, R.S. Influence of geometric scaling on the stability and range of a turbocharger centrifugal compressor. In Proceedings of the ASME Turbo Expo 2005: Power for Land, Sea, and Air, Reno, NV, USA, 6–9 June 2005.
18. Bell, D.; Zimmerle, D.; Bradley, T.; Olsen, D.; Young, P. Scalable turbocharger performance maps for dynamic state-based engine models. *Int. J. Engine Res.* **2016**, *17*, 705–712. [CrossRef]
19. Office of Energy Efficiency and Renewable Energy. Types of Fuel Cells. Available online: <https://www.energy.gov/eere/fuelcells/types-fuel-cells> (accessed on 25 April 2018).
20. Fuelcell.co.uk, 2000. Available online: <http://www.fuelcell.co.uk/proton-exchange-membrane-fuel-cells/> (accessed on 23 April 2018).
21. Bossel, U. Rapid startup SOFC modules. *Energy Procedia* **2012**, *28*, 48–56. [CrossRef]
22. Nissan Unveils World's First Solid-Oxide Fuel Cell Vehicle, Nissan Newsroom, August 2016. Available online: <https://newsroom.nissan-europe.com/uk/en-gb/media/pressreleases/148584/nissan-unveils-worlds-first-solid-oxide-fuel-cell-vehicle1> (accessed on 15 May 2018).
23. Steve Barrett, Toyota Begins Sales of Sora Fuel Cell Bus, Fuel Cells Bulletin, Volume 2018, April 2018. Available online: <https://www.sciencedirect.com/journal/fuel-cells-bulletin/vol/2018/issue/4> (accessed on 5 June 2018).
24. Badwal, S.P.S.; Giddey, S.; Kulkarni, A.; Goel, J.; Basu, S. Direct ethanol fuel cells for transport and stationary applications—A comprehensive review. *Appl. Energy* **2015**, *145*, 80–103. [CrossRef]
25. Ceres Power Unveils Latest SteelCell®Advances at Fuel Cell Expo, CeresPower. Available online: <http://www.cerespower.com/news/latest-news/ceres-power-unveils-latest-steelcell-advances-at-fuel-cell-expo/> (accessed on 2 July 2018).
26. Itoga, M.; Hamada, S.; Mizuno, S.; Nishiumi, H.; Murata, K.; Tonuma, T. Development of Fuel Cell Stack for New FCV. *SAE Tech. Pap.* **2016**, *1*, 0529.
27. Progress in Fuel Cell mCHP. Available online: <http://www.h2fcsupergen.com/wp-content/uploads/2013/06/Progress-in-Fuel-Cell-mCHP-Prof-Nigel-Brandon-Imperial.pdf> (accessed on 13 July 2018).
28. Yu, W.; Sichuan, X.; Ni, H. Air compressors for fuel cell vehicles: An systematic review. *SAE Int. J. Alt. Power.* **2015**, *4*, 115–122. [CrossRef]
29. Walters, M.; Wick, M.; Pischinger, S.; Ogrzewalla, J.; Sehr, A.; Tinz, S. *Fuel Cell System Development: A Strong Influence on FCEV Performance*; SAE Technical Paper; SAE International: Warrendale, PA, USA, 2018.
30. Hasegawa, T.; Imanishi, H.; Nada, M.; Ikogi, Y. *Development of the Fuel Cell System in the Mirai FCV*; SAE Technical Paper; SAE International: Warrendale, PA, USA, 2016.
31. Ricardo, M.B.; Apostolos, P.; Yang, M.B. Overview of Boosting Options for Future Downsized Engines. *Sci. China Technol. Sci. J.* **2011**, *54*, 318–331. [CrossRef]
32. Feneley, A.J.; Pesiridis, A.; Andwari, A.M. Variable geometry turbocharger technologies for exhaust energy recovery and boosting—A Review. *Renew. Sustain. Energy Rev.* **2017**, *71*, 959–975. [CrossRef]
33. Fischer, T.; Willers, O.W.; Seume, J.R. Preliminary design of a partial admission turbine for waste heat recovery in fuel cells. In Proceedings of the 13th International Conference on Turbochargers and Turbocharging Conference Proceedings, London, UK, 16–17 May 2018; ISBN 978-0-9956263-3-1.

34. Saisirirata, P. The solid oxide fuel cell (SOFC) and gas turbine (GT) hybrid system numerical model. *Energy Procedia* **2015**, *79*, 845–850. [CrossRef]
35. Assessment of Solid Oxide Fuel Cell Power System for Greener Commercial Aircraft, 2011. Available online: https://www.hydrogen.energy.gov/pdfs/progress11/x_10_chick_2011.pdf (accessed on 13 July 2018).
36. McPhail, S.J.; Aarva, A.; Devianto, H.; Bove, R.; Morenoa, A. SOFC and MCFC: Commonalities and opportunities for integrated research. *Int. J. Hydrogen Energy* **2011**, *36*, 10337–10345. [CrossRef]
37. Park, S.K.; Kim, T.S. Comparison between pressurized design and ambient pressure design of hybrid solid oxide fuel cell–gas turbine systems. *J. Power Sources* **2006**, *163*, 490–499. [CrossRef]
38. Buonomano, A.; Calise, F.; d’Accadia, M.D.; Palombo, A.; Vicidomini, M. Hybrid solid oxide fuel cells–gas turbine systems for combined heat and power: A review. *Appl. Energy* **2015**, *156*, 32–85. [CrossRef]
39. Itoga, M.; Hamada, S.; Mizuno, S.; Nishiumi, H.; Murata, K.; Tonuma, T. *Development of Fuel Cell Stack for New FCV*; SAE International: Warrendale, PA, USA, 2016.
40. Johnson, K.; Veenstra, M.J.; Gotthold, D.; Simmons, K.; Alvine, K.; Hobein, B.; Houston, D.; Newhouse, N.; Yeggy, B.; Vaipan, A.; et al. Advancements and Opportunities for On-Board 700 Bar Compressed Hydrogen Tanks in the Progression Towards the Commercialization of Fuel Cell Vehicles. *SAE Int. J. Alt. Power* **2017**, *6*, 201–218. [CrossRef]
41. Hong, D.K.; Woo, B.C.; Jeong, Y.H.; Koo, D.H.; Cho, Y.H. The performance analysis of ultra-high speed PM type synchronous motor-generator for micro turbine. *World Sci. Adv. Mater. Dev. Perform.* **2011**. [CrossRef]
42. Nissan e-NV200 Combi, Electric Vehicle Database. Available online: <https://ev-database.uk/car/1117/Nissan-e-NV200-Combi> (accessed on 1 August 2018).
43. Nissan’s Bio-Ethanol Fuel-Cell EV with 600km Range, Nissan Motor Corporation, August 2016. Available online: <https://reports.nissan-global.com/EN/?p=17768> (accessed on 7 August 2018).
44. Statistiques Sur Les Prix de l’électricité, Eurostat, June 2017. Available online: http://ec.europa.eu/eurostat/statistics-explained/index.php?title=Electricity_price_statistics/fr (accessed on 19 August 2018).
45. Hydrogène: Air Liquide Inaugure une Nouvelle Station à Orly, Automobile Propre, December 2017. Available online: <http://www.automobile-propre.com/hydrogene-air-liquide-inaugure-nouvelle-station-orly/> (accessed on 19 August 2018).



© 2018 by the authors. Licensee MDPI, Basel, Switzerland. This article is an open access article distributed under the terms and conditions of the Creative Commons Attribution (CC BY) license (<http://creativecommons.org/licenses/by/4.0/>).